Flow Turbulence Combust (2013) 90:681–707
DOI 10.1007/s10494-012-9394-z

New Directions in Advanced Modeling and in Situ Measurements Near Reacting Surfaces

John Mantzaras

Received: 25 May 2011 / Accepted: 14 March 2012 / Published online: 26 February 2013

Abstract Multidimensional numerical modeling and in situ spatially-resolved measurements of gas-phase thermoscalars over the catalyst boundary layer have fostered fundamental investigation of the heterogeneous and homogeneous chemical reaction pathways and their coupling at realistic operating conditions. The methodology for validating catalytic and gas-phase reaction mechanisms is firstly outlined for industrially-relevant fuels. Combination of advanced modeling and in situ near-wall species and velocity measurements is then used to address the intricate interplay between interphase fluid transport (laminar or turbulent) and hetero-/homogeneous kinetics. Controlling parameters of this interplay are the homogeneous ignition chemistry, flame propagation characteristics, competition between the catalytic and gaseous pathways for fuel consumption, diffusional imbalance of the limiting reactant, flow laminarization due to heat transfer from the hot catalytic walls, and fuel leakage through the gaseous reaction zone. Dynamic reactor operation and intrinsic flame dynamics driven by interactions between homogeneous kinetics and catalytic walls are outlined using detailed transient simulation. It is shown that the presence of catalytic reactions moderates flame instabilities. Future directions for transient modeling and for temporally-resolved in situ near-wall measurements are finally summarized.

Keywords Hetero-/homogeneous combustion modeling · Near-wall in situ Raman · LIF and PIV measurements · Homogeneous ignition over catalytic surfaces · Turbulent channel flow catalytic combustion · Flame dynamics in catalytic channels

Nomenclature

B	ratio of catalytically active to geometrical surface area
c_p, c_s	Specific heat of gas at constant pressure, specific heat of solid

J. Mantzaras (✉)
Paul Scherrer Institute, Combustion Research, 5232 Villigen PSI, Switzerland
e-mail: ioannis.mantzaras@psi.ch

D_k^T	Thermal diffusion coefficient of k-th species
D_{km}	Mixture average species diffusion coefficient of k-th species
f_μ	Turbulent damping function
H	Channel height
h	Total enthalpy
$\underline{\underline{\mathrm{I}}}$	Unity matrix
$\tilde{k}$	Turbulent kinetic energy
k_s	Thermal conductivity of solid
K_g, K_s	Number of gas-phase species, number of surface species
K_b	Number of bulk species
M	Sum of K_s and K_b for a given surface phase
Le	Lewis number (thermal over species diffusivity)
p	Pressure
$\dot{q}_{rad}$	Surface radiation flux
R^o	Universal gas constant
Re_{IN}	Inlet Reynolds number
$\dot{s}_k$	Heterogeneous molar production rate of k-th species
$\tilde{S}_\varphi$	Source term for variable φ in turbulent transport equations
T	Temperature
u, v	Streamwise and transverse velocity
U_{IN}	Inlet streamwise velocity
$\vec{V}_k$	Diffusion velocity vector for k-th gaseous species
$W_{k,}$, $\bar{W}$	Molecular weight of k-th species, average molecular weight
Y_k	Mass fraction of k-th gaseous species

Greek Symbols

Γ	Surface site density
Γ_ℓ, Γ_{eff}	Laminar and effective turbulent transport coefficients
$\tilde{\varepsilon}$	Dissipation rate of turbulent kinetic energy
θ_m	Coverage of m-th surface species
λ_g	Thermal conductivity of the gas
μ, μ_t	Viscosity, turbulent viscosity
ρ, ρ_s	Gas density, solid density
σ_m	Surface species site occupancy
φ	Equivalence ratio, thermoscalar variable
$\dot{\omega}_k$	Gas-phase species molar production rate

Turbulence Averaging

$\sim$, $-$	Favre- and Reynolds-averaging

Abbreviations

DNS	Direct numerical simulation
GHSV	Gas hourly spatial velocity
LR	Low Reynolds number

1 Introduction

Heterogeneous (catalytic) or combined heterogeneous and homogeneous (gas-phase) chemical processes are of interest in numerous industrial applications that include fuel reforming and synthesis, fuel cells, exhaust gas treatment in internal combustion engines, microreactors for portable heat and power generation, industrial and household burners, and gas turbines for large-scale power generation. Improvement of such systems crucially depends on the development of new catalysts with enhanced reactivity/selectivity/stability, understanding of the fundamental physicochemical processes at or above the catalyst surfaces, and advancement in multidimensional modeling. Numerical models, in particular, should have adequate description of the underlying heterogeneous and low-temperature homogeneous chemistry, and realistic interphase and intraphase fluid transport. There is currently an ever-increasing need for hetero-/homogeneous chemical reaction schemes valid over extended operating ranges; for example, heat or power generation systems encompass pressures from 1 bar in household burners to 3–5 bar in microreactors [1, 2] and to 20 bar in large stationary gas turbines [3, 4].

Advances in surface science measuring techniques [5, 6] have aided the development of detailed catalytic reaction mechanisms by identifying the relevant elementary reaction pathways and surface species. However, as most surface science data pertain to ultrahigh vacuum (UHV) and single-crystal surfaces, extension of the resulting reaction mechanisms to realistic pressures and technical catalysts (polycrystalline surfaces and supported catalysts) is not warranted. Hence there is need for additional validation tools, which are largely based on measurements of gas-phase thermoscalars in laboratory-scale reactors. To bridge the pressure and materials gap between surface science and technical catalysis, in situ spatially-resolved measurements of major and minor gas-phase species concentrations over the catalyst boundary layer by means of spontaneous Raman and laser induced fluorescence (LIF), respectively, have recently fostered fundamental hetero-/homogeneous kinetic studies at elevated pressures and temperatures, realistic reactant compositions, and technical catalyst surfaces [7–11]. It is emphasized that gas-phase chemistry cannot always be ignored, particularly at elevated pressures, even at the very large geometrical confinements (large surface-to-volume ratios) of typical catalytic reactors [10].

Advanced numerical modeling is needed not only for understanding the fundamental hetero-/homogeneous combustion processes but also for reactor design. The latter is compounded by the complex catalytic reactor geometry, which in many cases comprises a honeycomb structure. The underlying physicochemical processes within each channel of a typical honeycomb structure are illustrated in Fig. 1. Catalytic ignition (light-off) is achieved at a location depending not only on the operating conditions and the specific catalyst formulation, but also on key heat transfer mechanisms such as heat conduction in the solid channel walls and surface radiation heat transfer [12, 13]. The catalytic conversion at light-off shifts from kinetically-controlled to transport-controlled and this is manifested by the practically zero concentration of the deficient reactant on the catalyst surfaces (see, for example, in Fig. 1 the fuel mass fraction, Y_F, profile for a fuel-lean reactive mixture). Catalytically-produced heat and combustion products diffuse back to the flow and under certain conditions homogeneous combustion may also be initiated (Fig. 1).

Four major coupling routes between the two reaction pathways affect the onset of homogeneous ignition. The near-wall catalytic depletion of the limiting reactant

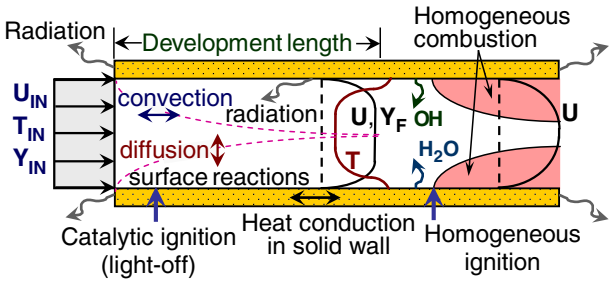

Fig. 1 Physicochemical processes occurring in a catalytic channel

inhibits homogeneous ignition, while heat transfer from the hot catalytic walls to the gas promotes homogeneous ignition [14, 15]. Gas-phase ignition is moderately inhibited by radical recombination reactions on the catalyst surface [9, 11, 16] and finally it can either be inhibited or promoted by heterogeneously-produced major species (notably H_2O or CO_2), depending on the fuel and operating conditions [9, 17, 18]. Figure 1 clearly demonstrates the need for advanced multidimensional modeling. Homogeneous ignition is strongly dependent on the boundary layer profiles of species and temperature and thus requires at least a 2-D model. Moreover, transient light-off studies are compounded by long integration times due to the slow thermal response of the solid; use of the quasisteady assumption for the gas cannot always be applied for model simplification, as will be discussed in Section 4.3.

It is demonstrated in this article that the combination of in situ measurements above the catalyst surface with multidimensional modeling can advance the development and/or refinement of catalytic and gas-phase chemical reaction schemes at industrially-relevant operating conditions. The methodology for the validation of hetero-/homogeneous chemical reaction schemes is presented in Section 4.1 for combustion of methane, propane and hydrogen over platinum at pressures up to 16 bar. Laminar or turbulent interphase transport (from the bulk of the gas to the outer catalyst surface) and its coupling to the hetero-/homogeneous chemistry is addressed in Section 4.2. It is shown that key for understanding this multifaceted coupling is the combination of in situ thermoscalar and velocity measurements near the reacting surface. New modeling and experimental directions in dynamic hetero-/homogeneous combustion systems are finally outlined in Section 4.3.

2 Experimental

Various reactor designs have so far been used for evaluating surface kinetics. A widely employed configuration is the nearly-isothermal, low temperature (typically less than 500°C), gradientless (in the cross-flow direction) microflow catalytic reactor [19, 20]; therein, the reactants are highly diluted with inert gases so as to minimize the combustion temperature rise. The composition at the exit of the reactor is monitored with mass spectrometry and/or gas chromatography. Even thought modeling of such reactors is simple, the isothermal operation may mask the description of certain reaction pathways that are thermally controlled. Moreover, high temperature studies are not possible, as they require excessive gas hourly spatial velocities (GHSV) to alleviate transport limitations. A final disadvantage of microflow reactors is that they

cannot account for the potential contribution of gaseous chemistry –an important issue at elevated pressures. Another devise commonly used for kinetic studies is the stagnation flow reactor, which has provided large databases on catalytic ignition and extinction, steady fuel conversion and product selectivity, under realistic operating conditions [21–24]. Stagnation-flow experiments have mostly yielded global parameters (total fuel conversion, product selectivity, autothermal behavior etc.), despite the fact that the geometry itself is amenable to spatially-resolved measurements.

A novel configuration for kinetic studies allowing for spatially resolved measurements is the high-pressure, high-temperature, optically accessible channel-flow reactor shown in Fig. 2 [8–11, 25, 26]. The test rig includes a rectangular reactor and a cylindrical steel tank providing pressurizations up to 20 bar. The reactor comprises two horizontal Si[SiC] non-porous ceramic plates (300 mm long, 104 mm wide, placed 7 mm apart) and two 3-mm-thick vertical quartz windows. The inner Si[SiC] surfaces are coated with the catalyst of interest, while the surface temperatures of both plates

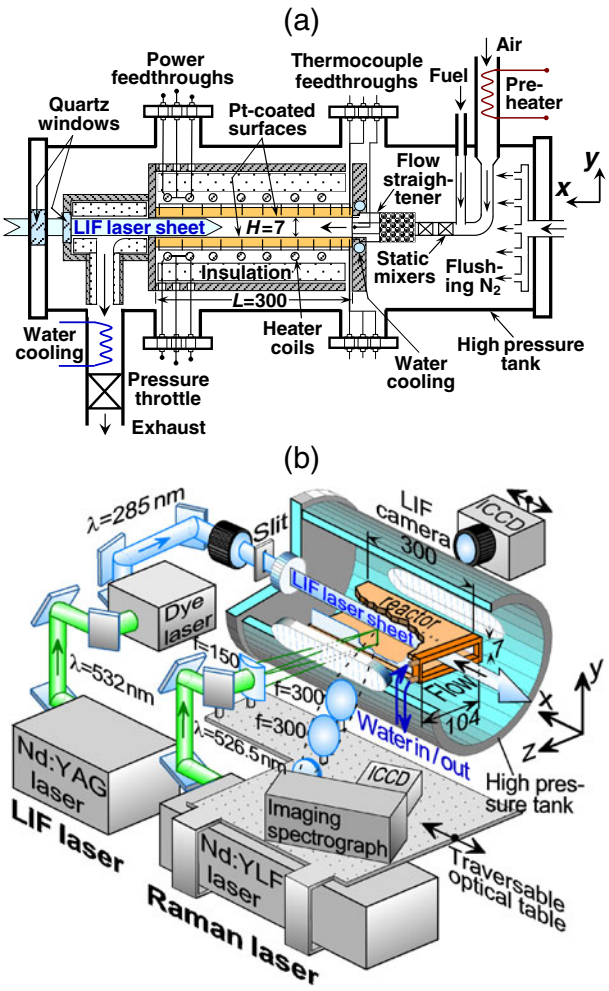

Fig. 2 **a** Schematic of catalytic channel-flow reactor and high-pressure test rig, and **b** optical arrangement of the Raman/OH-LIF setup [11]. All distances are in mm

are monitored with thermocouples (12 for each plate) positioned along the x-y streamwise symmetry plane and embedded 0.9 mm beneath the catalyst surfaces. To establish finite-rate catalytic reactant conversion and/or onset of homogeneous ignition, the surface temperatures are controlled by a cooling/heating arrangement: the front facets of the ceramic plates are contacted to a water-cooled support metal frame while two resistive heaters are positioned above the outer ceramic plate surfaces (see Fig. 2a).

Optical accessibility is maintained from both reactor sides via two 35-mm-thick high pressure quartz windows on the tank; furthermore, a counterflow streamwise optical access is also available through a rear tank flange. Non-intrusive, in situ, laser-based spectroscopic techniques are applied, shown in their latest configuration [25–27] in Fig. 2b. Measurements include 1-D spontaneous Raman of major gaseous species concentrations and temperature across the entire channel height ($H = 7$ mm) using an Nd:YLF laser, and planar laser induced fluorescence (LIF) of trace species (typically OH or CH_2O) along the x-y symmetry plane with a tunable dye laser pumped by an Nd:YAG laser. Absolute OH signals can be deduced via absorption calibration measurements carried out through the side optical windows (z-direction in Fig. 2b), as discussed in [8]. Kinetic studies are performed at steady and laminar flow conditions, with incoming Reynolds numbers (based on the channel height H) of less than 1000. Given the steady and laminar operating conditions, Raman scattered light from 240,000 to 480,000 pulses is integrated on the detector chip to increase the signal-to-noise ratio. Laser repetition rate, number of integrated pulses and temporal width of the camera intensifier gate are chosen to optimize the signal-to-noise ratio. Similarly, for the LIF experiments 400 to 1200 images are averaged to increase the signal-to-noise ratio.

Turbulent transport (of interest to gas turbine applications) can also be assessed by combining Raman/LIF and particle image velocimetry (PIV) [28]. Consequently, both chemistry and interphase transport can be assessed in this reactor configuration.

The reactor in Fig. 2 has a number of advantages originating either from its geometry or from the in situ and spatially-resolved nature of the measurements. Because large transverse (y-direction) gradients can be tolerated, catalytic reactivity studies can be performed at high surface temperatures (e.g. up to 1400 K), without the need for excessively large GHSV. Moreover, the reactor is suitable for investigating combined hetero-/homogeneous processes, since LIF of radicals allows for monitoring gaseous combustion. The aforementioned benefits come at an increasing experimental complexity and numerical cost. Multidimensional reactive CFD models, discussed in the next section, are required to simulate the experiments in this reactor.

3 Numerical

Spatially multidimensional models are herein considered given the fact that, as discussed in the previous section, 1-D models cannot correctly account for the onset of homogeneous ignition. Furthermore, although for a pure catalytic system (absence of gaseous reactions) 1-D models are appealing for their simplicity, unique lumped heat and mass transport coefficients (Nusselt and Sherwood numbers) are not guaranteed for the entry channel-flow problem in Fig. 1 in the presence of non-uniform wall temperature and surface reactions [29]. The governing equations for

hetero-/homogeneous reacting systems (such as the ones shown in Figs. 1 and 2) are presented next in vectorial form, appropriate for 2-D and 3-D geometries in any coordinate system.

Continuity equation:

$$\frac{\partial \rho}{\partial t} + \nabla \cdot (\rho\, \vec{u}) = 0. \tag{1}$$

Momentum equations:

$$\frac{\partial (\rho \vec{u})}{\partial t} + \nabla \cdot (\rho\, \vec{u}\vec{u}) + \nabla p - \nabla \cdot \mu \left[\nabla \vec{u} + (\nabla \vec{u})^T - \frac{2}{3} (\nabla \cdot \vec{u}) \underline{\underline{I}} \right] = 0. \tag{2}$$

Total enthalpy equation:

$$\frac{\partial (\rho h)}{\partial t} + \nabla \cdot (\rho\, \vec{u}\, h) + \nabla \cdot \left(\sum_{k=1}^{Kg} \rho Y_k h_k \vec{V}_k - \lambda_g \nabla \right) = 0. \tag{3}$$

Gas phase species equations:

$$\frac{\partial (\rho Y_k)}{\partial t} + \nabla \cdot \rho Y_k (\vec{u} + \vec{V}_k) - \dot{\omega}_k W_k = 0, k = 1, .., \ Kg. \tag{4}$$

Buoyancy is usually neglected in Eq. 2, given the small channel hydraulic diameters and the horizontal flow direction for most industrial applications , while gas-phase radiation is not considered in Eq. 3 given the small optical paths of catalytic channels. It is understood that second derivatives along the streamwise direction are also retained in Eqs. 2–4, leading to a full elliptic (Navier Stokes) model description. Parabolic (boundary layer) flow models are computationally much more efficient than elliptic ones, however, care must be exercised in their use due to flame-induced appreciable streamwise gradients. Criteria for the applicability of parabolic models in hetero-/homogeneous channel combustion have been established in Mantzaras et al. [30].

The surface species coverage, for a reaction scheme that conserves surface sites, is:

$$\frac{\partial \theta_m}{\partial t} = \sigma_m \frac{\dot{s}_m}{\Gamma}, \ m = 1, \ldots, \ K_s. \tag{5}$$

Finally, the ideal and caloric gas laws close the system of equations:

$$p = \rho R^o T / \bar{W} \text{ and } h_k = h_k^o(T_o) + \int_{T_o}^{T} c_{p,k} dT, , \ k = 1, .., \ Kg. \tag{6}$$

The diffusion velocities $\vec{V}_k$ in Eqs. 3 and 4 are generally computed using mixture average diffusion including thermal diffusion for the light species [31]:

$$\vec{V}_k = -D_{km} \nabla \left[\ln \left(Y_k \bar{W} / W_k \right) \right] + \left[D_k^T W_k / (\rho Y_k \bar{W}) \right] \ \nabla \ (\ln T). \tag{7}$$

The interfacial gas-phase species boundary conditions are:

$$\left[\rho Y_k (\vec{V}_k + \vec{u}_{st}) \right]_+ \cdot \vec{n}_+ = B \ W_k \dot{s}_k, \tag{8}$$

with $\vec{n}_+$ the outward-pointing normal to the catalytic walls, $\vec{u}_{st}$ the Stefan velocity $\left(= \frac{1}{\rho} \sum_{k=1}^{K_g} W_k \dot{s}_k\right)$, and "+" denoting gas properties just above the gas-wall interface. The factor B in Eq. 8 is the ratio of the catalytically active area to the geometrical surface area. Intraphase diffusion (gaseous species diffusion inside the porous catalyst washcoat) is herein not considered, as the experiments presented in this article refer to either polycrystalline noble metal catalysts on non-porous catalyst supports. Intraphase diffusion models have been assessed in [32].

A multidimensional model for heat transfer in the solid wall is also considered, given the rise of significant temperature gradients in the normal to the catalyst direction during transient reactor operation [33]:

$$\frac{\partial(\rho_s c_s T_s)}{\partial t} - \nabla \cdot (k_s \nabla T_s) = 0, \tag{9}$$

with interfacial energy boundary condition:

$$\left[-\lambda_g \nabla T + \vec{\dot{q}}_{rad}\right]_+ \cdot \vec{n}_+ + (k_s \nabla T_s)_- \cdot \vec{n}_+ + B \sum_{k=1}^{K_g+M} h_k \dot{s}_k W_k = 0. \tag{10}$$

Finally, the system of equations must be supplemented with proper initial and boundary conditions at the inlet, outlet, and the external solid wall surfaces, which depend on the specific application. Equations 1–10 describe all underlying processes in the channel of Fig. 1 and resolve all relevant spatiotemporal scales. As such, the solution of Eqs. 1–10 is also referred to as direct numerical simulation (DNS) irrespective of the flow condition (laminar or turbulent). Suffice it to say that the full model of Eqs. 1–10 must be elliptic in nature, since parabolic marching solvers do not allow for upstream propagation of heat via conduction in the solid and surface radiation (see Eqs. 9 and 10).

For the laboratory channel reactor in Fig. 2, the numerical model is simplified since kinetic studies are performed at steady-state and the interfacial energy boundary condition is prescribed wall temperature:

$$T(x, y = 0) = T_{w,l}(x), \;\; T(x, y = H) = T_{w,u}(x), \tag{11}$$

with $T_{w,u}(x)$ and $T_{w,l}(x)$ the temperature profiles of the upper and lower wall, respectively, fitted through the 12 thermocouple measurements of each plate (see Fig. 2a). Since the boundary condition in Eq. 11 negates modeling of solid heat conduction and surface radiation, computationally efficient parabolic solvers can now be used, however, under the restrictions discussed in [30].

4 Results and Discussion

4.1 Assessment of catalytic and gas-phase reaction mechanisms

Evaluation of catalytic and gaseous kinetics is presented in this section for fuel-lean combustion of CH_4, C_3H_8 and H_2 over polycrystalline platinum. The catalytic reactivity is firstly assessed using Raman measurements and homogeneous combustion is subsequently evaluated using both Raman and OH-LIF data. The methodology is

benchmarked in some detail with the combustion of fuel-lean methane/air mixtures (equivalence ratios $\varphi \leq 0.4$) at pressures up to 16 bar. Propane and hydrogen studies are subsequently presented to demonstrate underlying differences between various heterogeneous and homogeneous reaction schemes.

The procedure for assessing the catalytic reactivity from the Raman data is demonstrated in Fig. 3. The initial step is to demarcate the reactor length over which the gaseous pathway has an insignificant contribution to the total methane conversion. Figure 3a provides the predicted catalytic (C) and gas-phase (G) methane axial conversion rates at a pressure of 4 bar; these quantities were computed using a 2-D steady-state variant of the full numerical model described in Section 3, with detailed heterogeneous and homogeneous reaction schemes (Deutschmann et al. [34] and Warnatz et al. [35], respectively). The volumetric G conversion rate in Fig. 3a has been integrated across the 7-mm channel height in order to facilitate comparisons with the surface C conversion rate. Appreciable gaseous methane conversion occurs downstream the location marked as x_{ag} in Fig. 3a, which is defined as the far upstream position whereby G amounts to 5% of C. This position is not always related to the onset of homogeneous ignition, since noticeable gaseous methane conversion can precede thermal runaway (via the incomplete oxidation of the hydrocarbon fuel to CO), with this effect being more pronounced at elevated pressures [10].

Measured transverse species profiles are compared against simulations in Fig. 3b only at $x < x_{ag}$ in order to avoid potential falsification of the catalytic kinetics by the gaseous chemistry. Essential for such comparisons is the attainment of kinetically controlled catalytic conversion, which is manifested in Fig. 3b by the non-zero concentrations of the limiting reactant (methane) at both channel walls ($y = 0$ and 7 mm). The slight asymmetry in the transverse species profiles is due to moderate

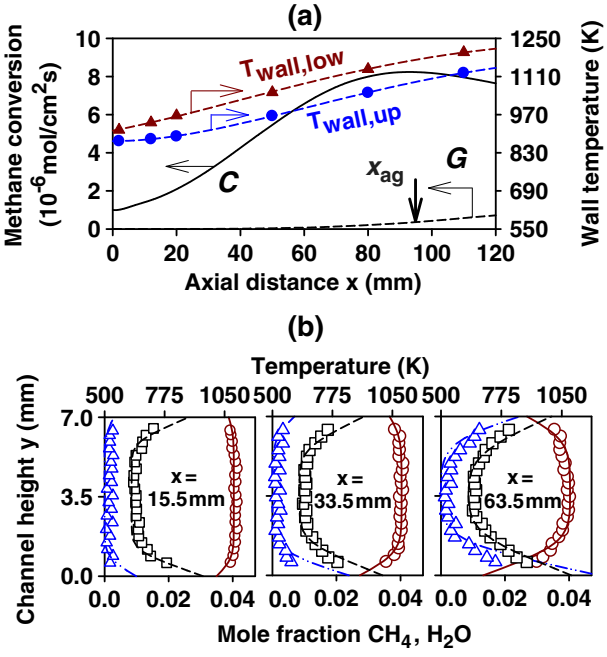

Fig. 3 Combustion of CH_4/air over platinum in the reactor of Fig. 2. **a** Computed axial profiles of catalytic (C) and gaseous (G) CH_4 conversions for $p = 4$ bar, $\varphi = 0.40$, $T_{IN} = 624$ K and $U_{IN} = 2.05$ m/s (adapted from [10]), and measured upper wall temperatures (*circles*) and lower wall temperatures (*triangles*). The *arrow* at x_{ag} marks the onset of appreciable gaseous contribution. **b** Computed (*lines*) and Raman-measured (*symbols*) transverse profiles: CH_4 (*circles*, *solid lines*), H_2O (*triangles*, *dashed-dotted lines*) and temperature (*squares*, *dashed lines*) at three selected axial positions $x < x_{ag}$

differences between the upper and lower wall temperatures, as seen by the measured temperature profiles in Fig. 3a. Measurements and simulations in Fig. 3b are in good agreement with each other. In particular, the predicted near-wall bending of the methane profile, which is in turn directly linked to the catalytic reactivity, is in very good agreement with the measurements, notwithstanding the lack of Raman data closer than 0.6 mm to both walls due to low signal-to-noise ratios.

The above comparisons have thus demonstrated the aptness of the employed catalytic reaction scheme; moreover, extensive studies have shown [10] that this catalytic scheme [34] is appropriate over the pressure and wall temperature ranges 1 bar $\leq p \leq$ 16 bar and 780 K $\leq T_w \leq$ 1250 K, respectively. Additional comparisons of the measurements with other catalytic reaction schemes have revealed [10] that the appropriate high pressure performance of any surface mechanism mainly reflects its capacity to capture the decrease in surface free site coverage with rising pressure; this process in turn restrains the rate of enhancement of the catalytic reactivity with increasing pressure. The catalytic reaction rate of methane has an overall pressure dependence p^{1-n}, where $0 < 1-n < 1$ with the exponent n actually being a function of pressure. The validity of the employed catalytic mechanism at high pressures is due to a methane adsorption rate that has an order of 2.3 with respect to the platinum free site coverage. Finally, the results (Fig. 3) have exemplified the importance of accurate near-wall species measurements. Therefore, lased-based spectroscopic techniques should aim in the future at improving the signal-to-noise ratios at distances increasingly closer to the catalyst surface (less than the presently feasible 0.6 mm). Construction of slightly curved catalytic surfaces, for example, can facilitate reliable measurements as close as 0.1 mm from the wall.

The assessment of gas-phase reaction schemes, which entails combination of OH-LIF and Raman data, is discussed next. An evaluation of the catalytic processes preceding the onset of homogeneous ignition is still essential, despite the previous validation of the catalytic scheme. The reason is that the higher surface temperatures required for homogeneous ignition may cause partial or total catalyst deactivation, resulting in a near-wall fuel excess that would in turn accelerate the onset of gas-phase ignition and thus falsify gaseous kinetics. This problem is further compounded by the existence of multiple combinations of catalytic and gaseous reactivities yielding exactly the same homogeneous ignition distance [14, 15], as illustrated in Fig. 4. Therein, infinite combinations of surface reactivities (characterized by a

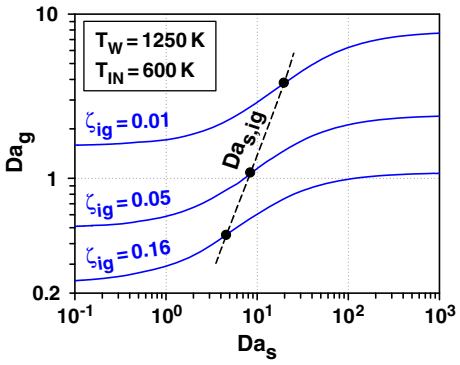

Fig. 4 Lines of constant non-dimensional homogeneous ignition distances (ζ_{ig}) for various combinations of catalytic (Da_s) and gas-phase (Da_g) Damköhler numbers, computed using the analytical ignition criterion established in [15] via matched activation energy asymptotics. The symbols mark the catalytic ignition (light-off) Damköhler numbers, $Da_{s,ig}$

surface Damköhler number, Da_s) and gas-phase reactivities (characterized by a gas-phase Damköhler number, Da_g) provide the same non-dimensional homogeneous ignition distance ζ_{ig}. Although the LIF-measured shape of the ensuing flame can be invoked to eliminate many of the theoretically possible Da_s and Da_g combinations, the Raman data provide the only unambiguous way of removing any uncertainties associated with the catalytic pathway that may affect the evaluation of gaseous chemistry.

Gas-phase combustion of methane over Pt has been studied over the ranges 1 bar $\leq p \leq$ 16 bar and 1050 K $\leq T_w \leq$ 1430 K [8, 11, 18, 36]. Measured and predicted 2-D distributions of the OH radical are compared in Fig. 5b for two cases at 6 and 16 bar. The location of homogeneous ignition (x_{ig}), marked with arrows in Fig. 5b, has been defined in both predictions and experiments as the far upstream location whereby OH reaches 5% of its maximum value in the reactor. Predicted and Raman-measured transverse species profiles for the 16 bar case of Fig. 5b are shown in Fig. 5a, indicating correct prediction of the catalytic processes over the gaseous induction zone (it is therein evident that the catalytic methane conversion is nearly transport-limited). The gaseous scheme of Warnatz et al. [35], amended in one reaction as described in [11], reproduces the measured homogeneous ignition position and the subsequent flame sweep angles (see Fig. 5b). It has been further shown [11] that other reaction mechanisms (GRI-3.0 [37] and Leeds [38]) under-predict considerably the measured x_{ig} at all pressures. Comprehensive analysis of the examined gaseous mechanisms shows [11] that the aforementioned differences are mainly an outcome of the low equivalence ratios and temperatures pertinent to the specific operating conditions of catalytic systems. In conclusion, the discussion in Figs. 3 and 5 has clearly demonstrated that in situ measurements of thermoscalars above catalyst surfaces can be used to assess the reactivity of both heterogeneous and homogeneous reaction pathways at industrially relevant operating conditions.

The hetero-/homogeneous chemistry coupling in terms of radicals and major species is briefly outlined, using the above-validated schemes of Deutschmann and modified-Warnatz. It has been shown [10, 11] that the catalyst itself is a poor source of OH radicals so as to meaningfully affect the gaseous pathway at conditions far

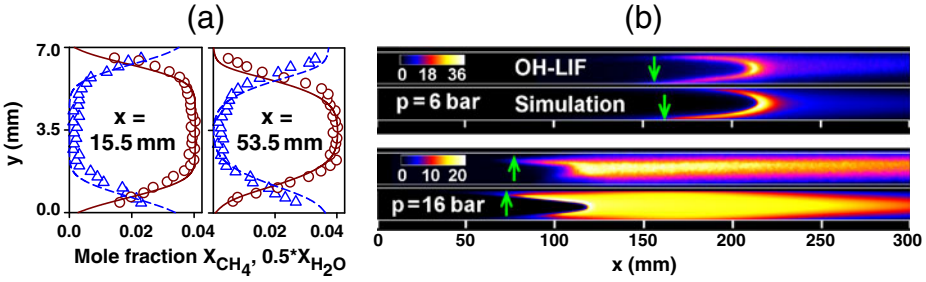

Fig. 5 Combustion of CH_4 over Pt. **a** Measured (*symbols*) and predicted (*lines*) transverse profiles of CH_4 (*circles*, *solid lines*) and H_2O (*triangles*, *dashed lines*) mole fractions for the 16 bar case in Fig. 5b, at two selected axial locations preceding the onset of homogeneous ignition (predictions using the Deutschmann/amended-Warnatz reaction schemes). **b** LIF-measured, and predicted OH maps for two cases: $p = 6$ bar, $\varphi = 0.36$, $T_{IN} = 569$ K, $U_{IN} = 0.43$ m/s and $p = 16$ bar, $\varphi = 0.40$, $T_{IN} = 643$ K and $U_{IN} = 0.45$ m/s. The arrows denote the onset of homogeneous ignition and the color bars provide the predicted OH in ppmv. Adapted from [11, 36]

from homogeneous ignition. On the other hand, at the downstream parts of the gaseous induction zone or at post-homogeneous-ignition zones, the catalyst turns to a sink of OH radicals. This behavior results in an overall mild inhibition of homogeneous ignition on radical (OH as well as O and H) reactions. In addition, it has been shown experimentally and numerically [18, 39] that the catalytically-produced water promotes chemically homogeneous ignition in methane combustion.

The Raman/OH-LIF methodology has been further applied to the hetero-/homogeneous combustion of fuel-lean ($\varphi \leq 0.43$) propane/air mixtures over Pt at pressures of up to 7 bar (pressure range of interest in microreactors) and temperatures 720 K $\leq T_w \leq$ 1280 K [40]. The fundamental issue under investigation is the pressure dependence of the catalytic reactivity. Simulations are performed using the atmospheric-pressure global catalytic mechanism of Garetto et al. [41], which is augmented with a pressure correction factor $(p/p_o)^{-n}$ in order to restrain the rate of increase of the catalytic reactivity with rising pressure, as also discussed in the foregoing methane studies.

$$\dot{s}_{C3H8} = A(p/p_o)^{-n}\, T_w^{1.15} \exp(-E_a/RT_w)\, \left[C_3H_8\right]_w^{\alpha}, \tag{12}$$

with $A = 93.2\ \mathrm{K}^{-1.15}\ \mathrm{cm}^{1.45}\ \mathrm{mol}^{-0.15}\ \mathrm{s}^{-1}$, $E_a = 71.128$ kJ/mole, $a = 1.15$ and $[C_3H_8]_w$ denoting the propane gas-phase concentration at the gas-wall interface.

Predicted and Raman-measured transverse profiles of propane and water mole fractions are presented in Fig. 6 for three different pressures and two selected axial positions for each pressure. The comparisons pertain to axial positions upstream of the onset of appreciable gas-phase propane conversion, in a manner analogous to the foregoing methane studies in Fig. 3. Comparison of simulations with the original scheme of Garetto et al. [41] (dashed lines for CH_4 in Fig. 6) indicate progressively

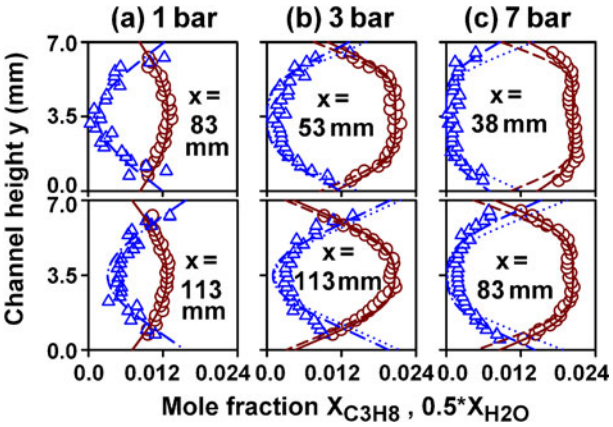

Fig. 6 Predicted (*lines*) and Raman-measured (*symbols*) transverse profiles of propane and water mole fractions at three pressures **a**: $p = 1$ bar, $\varphi = 0.30$, **b** $p = 3$ bar, $\varphi = 0.27$, and **c** $p = 7$ bar, $\varphi = 0.26$. Measurements: C_3H_8 (*circles*), H_2O (*triangles*). Predictions: C_3H_8 (*solid lines*: pressure-corrected reaction in Eq. 12; *dashed lines*: original reaction of Garetto et al. [41]), H_2O (*dashed-dotted lines*: pressure-corrected reaction; *dotted lines*: original reaction of Garetto et al. [41]). Adapted from [40]

increasing deviations with rising pressure, clearly showing that great care is needed when extrapolating atmospheric pressure catalytic kinetic data to elevated pressures. A pressure exponent $n = 0.4 \pm 0.03$ in Eq. 12 provides the best fit to the Raman-measured boundary layer propane profiles (see solid lines in Fig. 6) over the entire pressure range $1 \leq p \leq 7$ bar. Thus, the overall pressure dependence of the catalytic reaction in Eq. 12 is 0.75 (given the pressure exponent of 1.15 due to $[C_3H_8]_w$). Since detailed heterogeneous mechanisms for combustion of higher hydrocarbons are still under construction, global steps such as Eq. 12 offer at this stage a much needed tool for engineering calculations. It has been thus demonstrated that situ species measurements extending only a few millimeters away from the catalytic surfaces can be successfully used for quantifying the catalytic reactivity of industrially-relevant fuels at practical pressures. Lastly, for the assessment of homogeneous propane chemistry, Raman and OH-LIF measurements have been employed in a fashion similar to the methane studies in Fig. 5. It was shown [40] that the optimized C_3 elementary gas-phase mechanism by Qin et al. [42] reproduced the OH-LIF measured onset of homogeneous ignition.

The final investigation in this section addresses fuel-lean ($\varphi \leq 0.32$) combustion of hydrogen/air mixtures over Pt at atmospheric pressure and temperatures 950 K $\leq T_w \leq$ 1220 K [9]. While the previous propane case study depicted key dependencies of the catalytic reactivity, the hydrogen study aims at exposing homogeneous combustion characteristics and their coupling to heterogeneous combustion. The water-cooling arrangement discussed in Section 2 (see Fig. 2) at the channel entry is pivotal in suppressing the superadiabatic surface temperatures that would otherwise appear in the catalytic combustion of the highly diffusionally imbalanced hydrogen limiting reactant [9, 12] (Lewis number, $Le_{H2} \approx 0.3$).

Predicted and LIF-measured 2-D maps of the OH radical are provided in Fig. 7b. Similar to the foregoing methane studies in Fig. 5, the Raman measurements shown in Fig. 7a reproduced the computed transverse profiles of major species over the

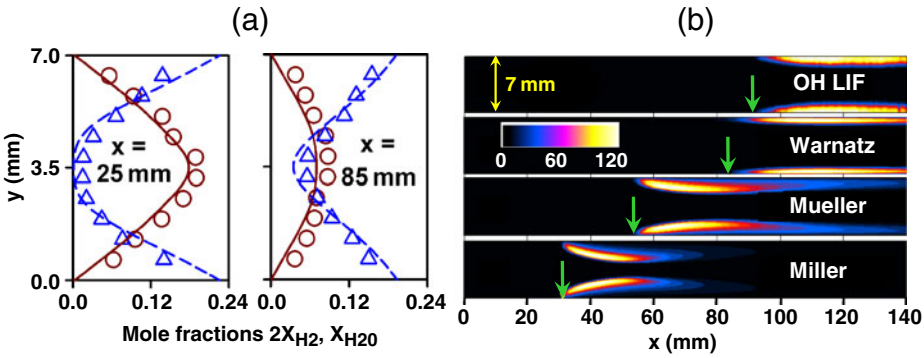

Fig. 7 Combustion of H_2 over Pt, $p = 1$ bar, $\varphi = 0.28$, $T_{IN} = 312$ K, $U_{IN} = 2$ m/s. **a** Measured (*symbols*) and predicted (*lines*) transverse profiles of H_2 (*circles*, *solid lines*) and H_2O (*triangles*, *dashed lines*) mole fractions at two selected axial locations preceding the measured onset of homogeneous ignition (adapted from [9]). **b** LIF-measured and numerically predicted distributions of the OH radical. Predictions with the catalytic scheme of Deutschmann et al. [22] and the gas-phase schemes of Warnatz et al. [35], Mueller et al. [43] and Miller and Bowman [44]. The arrows denote the onset of homogeneous ignition. The color bar provides the OH in ppmv

gas-phase induction zone (a transport-limited conversion of hydrogen is attested in Fig. 7a). Simulations are carried out using the catalytic scheme of Deutschmann et al. [22] and three different gas-phase schemes: Warnatz et al. [35], Mueller et al. [43] and Miller and Bowman [44]. The scheme from Warnatz mildly under-predicts the measured homogenous ignition distance, while the other two gaseous schemes lead to considerably shorter ignition distances. The significant differences between the performance of the various gaseous schemes, even for this simpler fuel in combustion, is largely attributed [9] to the catalytically-produced water, which is a very efficient third body in the chain terminating step $H+O_2+M = HO_2+M$. Therefore, any appropriate gas-phase mechanism in hetero-/homogeneous H_2 combustion must include proper third body efficiency for the water in this key reaction.

The difference in flame shapes between H_2 and CH_4 combustion (see Figs. 5b and 7b) is due to the low Lewis number of the former: hydrogen is transported more efficiently towards the near-wall hot ignitable zone than heat is transferred away from it, resulting in the confinement of the gaseous combustion zone close to the wall and in the formation of two separate flame branches. It is finally stressed that the discrepancies in effective ignition delay times between the different gaseous schemes in Fig. 7b (evaluated using the ignition distances and the flow velocities) can be as large as 20 ms, a particularly long time for practical systems (i.e. gas turbines using the catalytically stabilized combustion approach). The correct prediction of homogeneous ignition is in turn crucial for the design of hydrogen-based catalytic reactors.

4.2 Interplay of transport and hetero-/homogeneous chemistry

The previous section focused on assessing the heterogeneous and homogeneous reaction pathways and aspects of their respective kinetic coupling. The interplay of transport and hetero-/homogenous combustion will be discussed in this section and the importance of in situ near-wall measurements in understanding this multifaceted interaction will be demonstrated. Two examples are herein presented; the first one in laminar and the second one in turbulent transport, both dealing with hydrogen combustion over Pt.

Laminar combustion of lean H_2/air mixtures over Pt is studied numerically and experimentally in the test rig in Fig. 2 at pressures up to 15 bar, $0.08 \leq \varphi \leq 0.30$ and mixture preheats, T_{IN}, up to 780 K [25, 26, 45]. The simulations employ the catalytic scheme of Deutschmann et al. [34] and the gas-phase mechanism of Li et al. [46]; the latter has been specifically constructed for elevated pressures. Measured and predicted OH distributions are provided in Fig. 8 for three cases at different pressures, all with high preheats in the range 653–679 K. The agreement between measured and predicted ignition distances and flame shapes in Fig. 8 is quite good. Moreover, Raman measurements over the gaseous induction zones are in good agreement with the predictions [26], demonstrating a transport-limited catalytic conversion of H_2, similar to the previous atmospheric pressure studies (see Fig. 7a). Nonetheless, gaseous combustion is suppressed at 15 bar (see Fig. 8(3a,3b)), and this is also largely the behavior for pressures higher than 12 bar [26]. The diminishing gas-phase combustion with rising pressure is further shown in Fig. 9, providing the predicted catalytic and gas-phase H_2 conversions for the three examined cases in Fig. 8.

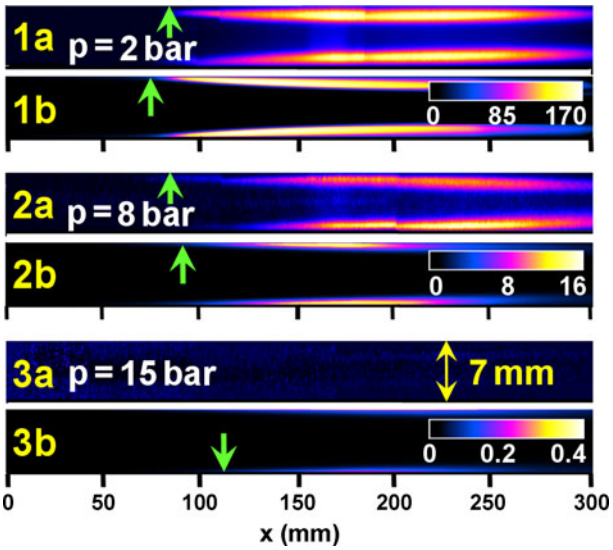

Fig. 8 LIF-measured **a** and predicted **b** distributions of the OH radical for H_2 combustion over Pt, for three cases: (1) $p = 2$ bar, $\varphi = 0.11$, $T_{IN} = 653$ K, (2) $p = 8$ bar, $\varphi = 0.11$, $T_{IN} = 676$ K, and (3) $p = 15$ bar, $\varphi = 0.11$, $T_{IN} = 679$ K. Predictions with the catalytic scheme of Deutschmann et al. [34] and the gas-phase mechanism of Li et al. [46]. The *arrows* denote the onset of homogeneous ignition and the color bars the predicted OH levels (ppmv). Adapted from [26]

To clarify the observed suppression of gaseous combustion with rising pressure, pure homogeneous ignition characteristics of hydrogen are initially investigated. Ignition delays of lean H_2/air mixtures ($\varphi = 0.10$ and 0.30) are computed in a constant pressure batch reactor and their inverses (quantities proportional to the gaseous reactivity) are plotted in Fig. 10a as a function of pressure with parameter the initial temperature. For a moderate batch reactor temperature of 1000 K (which, for the spatially inhomogeneous reactor in Fig. 2, represents an average between the inlet and the wall temperature with added weight on the latter), the gaseous reactivity initially decreases rapidly with rising pressure, while above 3 bar it only changes modestly. For $T > 1000$ K, the reactivity initially increases with rising pressure and then drops, with the turning point shifted to higher pressures for higher temperatures.

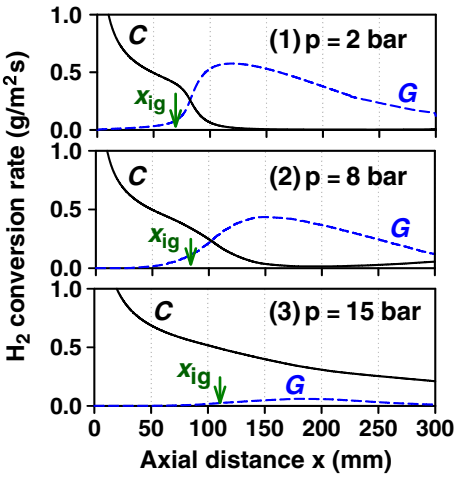

Fig. 9 Computed axial profiles of catalytic (C) and gaseous (G) hydrogen conversions for the three cases in Fig. 8. The *arrows* denote the onset of homogeneous ignition (adapted from [26])

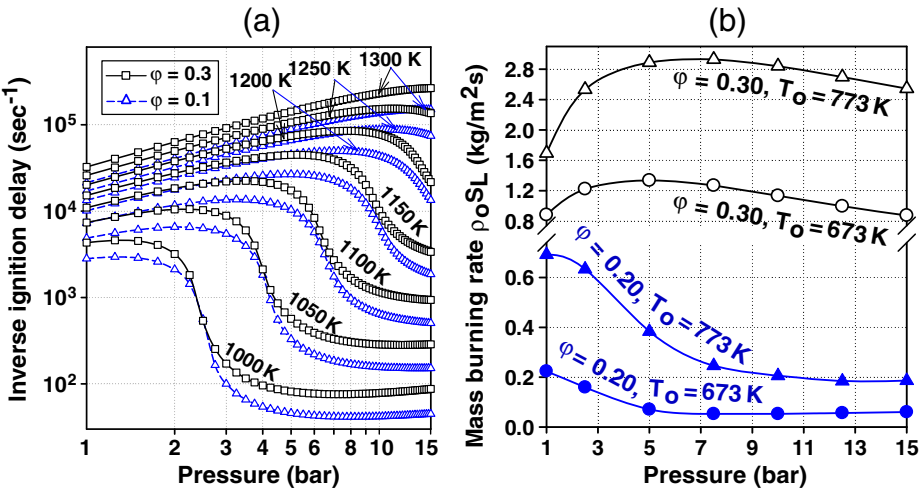

Fig. 10 **a** Computed inverse ignition delays of H_2/air mixtures ($\varphi = 0.30$ and 0.10) in a batch reactor at different pressures and temperatures. **b** Computed 1-D laminar burning rates versus pressure for H_2/air mixtures with $\varphi = 0.30$ and 0.20 and upstream temperatures $T_o = 673$ and 773 K (adapted from [26])

This rich behavior of H_2 gaseous ignition characteristics is caused by the competition between the chain branching step $H+O_2 \Leftrightarrow O+OH$, the chain terminating step $H+O_2+M \Leftrightarrow HO_2+M$, and the chain branching sequence $HO_2+H_2 \Leftrightarrow H_2O_2+H$ and $H_2O_2+M \Leftrightarrow 2OH+M$ that overtakes the stability of HO_2 in the termination step [47]. The implication for a hetero-/homogeneous reactor operating at moderate effective temperatures (ca. 1000 K) is that at sufficiently high pressures the catalytic pathway has the opportunity to consume significant amounts of H_2 during the elongated gas-phase induction zones, thus depriving fuel from the gaseous pathway and inhibiting homogeneous ignition. It is emphasized that the catalytic pathway is very effective in converting H_2 due to the large molecular diffusivity of this species and its very high reactivity on platinum even at moderate temperatures. Therefore, suppression of gaseous combustion at modest reactor temperatures and elevated pressures is a main result of competition between the two reaction pathways for fuel consumption. This picture can explain the hetero-/homogeneous combustion behavior for non-preheated H_2/air mixtures ($T_{IN} \approx 300$ K) reported earlier in Mantzaras et al. [45] and the associated suppression of gaseous combustion even at pressures as low as 4 bar.

For the preheated reactant experiments in Fig. 8, gas-phase combustion could not be sustained at $p > 12$ bar even at preheats as high as 780 K [26] (see e.g. the $p = 15$ bar case in Figs. 8 and 9). This may appear surprising, since for such high preheats, and for measured wall temperatures about 1200 K, the corresponding behavior in Fig. 10a (temperatures above 1150 K) indicates for $p > 12$ bar either a modest drop or a small increase in reactivity with rising pressure. However, the controlling parameter in this high preheat/pressure regime is not only ignition chemistry but also flame propagation characteristics. Laminar burning rates for 1-D freely propagating flames are plotted as a function of pressure in Fig. 10b for two H_2/air equivalence

ratios, $\varphi = 0.30$ and 0.20, and two mixture preheats, $T_o = 673$ K and 773 K; this is to mimic the increase in mixture preheat and drop in hydrogen content with increasing axial distance along the catalytic channel. For $T_o = 673$ K and $\varphi = 0.30$, the burning rate at 15 bar is 34% lower than the corresponding peak value at ∼5 bar, while for $T_o = 673$ K and $\varphi = 0.20$ the burning rate at 15 bar is 73% lower than the peak value at 1 bar; similar trends are evident for $T_o = 773$ K. The drop in laminar burning rates at the higher pressures leads to a push of the gaseous reaction zone closer to the wall, then to an increased leakage of hydrogen through the gaseous reaction zone (resulting in catalytic conversion of the escaped fuel at the wall) and finally to flame extinction. Therefore, the observed significant suppression of gaseous combustion at $p > 12$ bar and high mixture preheats bears the combined effects of the reduced laminar burning rates and also of the high molecular transport (low Lewis number) of hydrogen that decreases the availability of fuel in the near-wall hot ignitable region. This mechanism also explains the opposite behavior of methane, whereby gas-phase combustion intensifies with rising pressure from 1 to 16 bar (see flames in Fig. 5b): methane is nearly diffusionally neutral ($Le_{CH4} \approx 1$), while its burning rate increases with rising pressure as $p^{0.5}$.

The lack of appreciable gas-phase hydrogen combustion in certain regimes of pressure and reactant preheat is of concern in reactor design. It has been shown [9, 48] that, contrary to many premises, the presence of a flame inside a hydrogen catalytic reactor is advantageous as it shields the catalytic surfaces from the hydrogen-rich channel core, thus reducing the heterogeneous conversion that in turn causes superadiabatic surface temperatures. The absence of this moderation can be of concern, particularly for reactor thermal management at elevated pressures, thus exemplifying the need for proper gaseous chemistry description when dealing with either hydrogen or hydrogen-rich fuels, such as syngases [27, 48].

Another prime example of coupling between transport and hetero-/homogeneous reactions is turbulent catalytic combustion. In catalytic reactors of large turbines operating at full load, the inlet Reynolds numbers in each individual honeycomb channel can reach 30,000. In entry channel flows with heat transfer from the wall to the flowing gas, which is relevant to catalytic combustion systems, the controlling parameters are the magnitude of the incoming turbulence and the flow laminarization due to the increase in molecular viscosity with rising gas temperature [49]. Direct numerical simulation (DNS) in the entry region of a heated pipe air-flow at a moderate Re_{IN} of 4300 [50] complemented with experiments, has led to the development of advanced low Reynolds (LR) number turbulence models with suitable damping functions for strongly heated and developing channel flows [49]. Turbulent models for hetero-/homogeneous combustion have followed suit in [28, 51, 52]: a moment closure approach is therein adopted, whereby the Favre-averaged transport equation of any gas-phase variable φ is given by:

$$\frac{\partial(\bar{\rho}\tilde{u}\tilde{\varphi})}{\partial x} + \frac{\partial(\bar{\rho}\tilde{v}\tilde{\varphi})}{\partial y} - \frac{\partial}{\partial x}\left(\Gamma_{\text{eff}}\frac{\partial\tilde{\varphi}}{\partial x}\right) - \frac{\partial}{\partial y}\left(\Gamma_{\text{eff}}\frac{\partial\tilde{\varphi}}{\partial y}\right) = \tilde{S}_{\varphi}, \tag{13}$$

$$\Gamma_{\text{eff}} = \Gamma_{\ell} + \mu_t/\sigma_{\varphi} \text{ and } \mu_t = c_{\mu} f_{\mu} \bar{\rho}\tilde{k}^2/\tilde{\varepsilon}. \tag{14}$$

For the catalytic reaction rates, the large thermal inertia of the solid wall suppresses the surface temperature fluctuations and eliminates the major reaction non-linearity, thus greatly simplifying the surface chemistry modeling [28].

Three different LR turbulence models have been tested in [28]: the two-layer model of Chen and Patel [53] developed for non-heated flows; the LR model of Ezato et al. [49] which is validated in strongly laminarizing heated channel flows; and the LR model of Hwang and Lin [54] that is developed for channel flows with and without heat transfer. Raman and OH-LIF measurements are carried out in H_2/air turbulent combustion over Pt at $p = 1$ bar, in a manner similar to the laminar studies of Section 4.1. Additionally, particle image velocimetry (PIV) provides the 2-D velocity field (the PIV laser sheet has the same orientation as the OH LIF excitation laser sheet in Fig. 2 [28]). The gas-phase scheme or Warnatz et al. [35], which has been validated in the laminar studies of Section 4.1, and the catalytic scheme of Deutschmann et al. [34] are used in the simulations.

Measured and predicted transverse profiles of the mean velocity $\tilde{U}$ and the turbulent kinetic energy $\tilde{k}$ are compared in Fig. 11a for two cases with comparable inlet Reynolds numbers, one non-reacting (Case 1, flow of air without hydrogen) and one reacting (Case 2, flow of hydrogen/air). In the non-reacting Case 1, the two-layer model [53] yields very good agreement with the measurements. The heat transfer models of Hwang and Lin [54] and particularly of Ezato et al. [49], noticeably overpredict (underpredict) $\tilde{U}\left(\tilde{k}\right)$ (see Fig. 11a, Case 1)). The last two models are thus overdissipative, clearly demonstrating the aptness of the two-layer model and the inapplicability of the heat transfer LR models in isothermal channel-flows. Conversely, for the reacting Case 2 in Fig. 11a the LR model of Ezato et al. [49] provides good agreement with the measured $\tilde{U}$ and $\tilde{k}$. The Hwang and Lin model [54], and to a greater extent the two-layer model [53], overpredict $\tilde{U}$ significantly; moreover, these models yield considerably higher near-wall $\tilde{k}$ (Fig. 11a, Case 2) that in turn

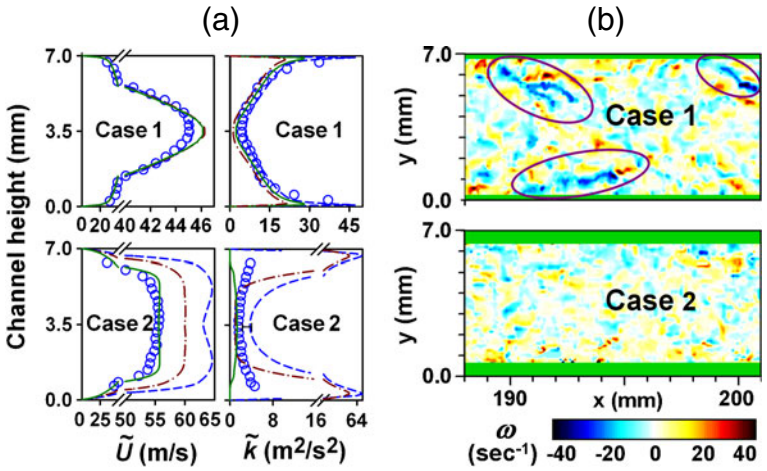

Fig. 11 **a** Transverse profiles of mean axial velocities $\tilde{U}$ and turbulent kinetic energies $\tilde{k}$ for the non-reacting Case 1 (300 K air-flow with $Re_{IN} = 35{,}240$) and the reacting Case 2 ($\varphi = 0.24$, $U_{IN} = 40$ m/s, wall temperatures up to 1220 K, $Re_{IN} = 30{,}150$), adapted from [28]. Symbols are measurements and lines are predictions with different LR turbulence models (*solid lines*: Ezato et al. [49]; *dashed-dotted lines*: Hwang and Lin [54]; *dashed lines*: Chen and Patel [53]). **b** PIV-measured instantaneous spanwise vorticity maps, for Cases 1 and 2. The encircled areas in Case 1 denote elongated vorticity structures. The blocked areas along both walls ($y = 0$ and 7 mm) indicate zones without PIV data

greatly enhances the transport of heat from the hot wall to the channel core, leading to an excessive acceleration of the mean flow $\tilde{U}$. Dampening of turbulence (laminarization) due to heat transfer is also evident from the PIV-measured instantaneous vorticity maps in Fig. 11b. High-vorticity elongated structures inclined at 40°–50° with respect to the flow direction are evident in the isothermal Case 1, as also reported in fully-developed isothermal turbulent channel flows [55]. On the other hand, for the reacting Case 2 the vortical structures are not only attenuated in magnitude but also lose their elongated topological features. In summary, from the tested heat-transfer LR models only Ezato et al. [49] provides a realistically strong turbulence damping for catalytic combustion applications.

Measured and predicted species distributions are compared in Fig. 12a for the reacting Case 2 and an additional reacting Case 3, with lower inlet Reynolds number. The model of Ezato et al. [49] provides good agreement to the Raman-measured species transverse profiles (Fig. 12a), while it has been shown [28] that the other two LR models overpredict appreciably the catalytic hydrogen conversion. The reason is that the latter models [53, 54] overpredict significantly $\tilde{k}$ (Fig. 11a) and hence the effective transport coefficient Γ_{eff} in Eq. 14, resulting in an increased transverse transport towards the wall and thus in a higher hydrogen catalytic consumption. It is emphasized that the catalytic chemistry is still fast enough to cope with the enhanced turbulent transport of these models (the catalytic conversion is transport-limited).

Finally, measured and predicted 2-D maps of the OH radical in Fig. 12b indicate that the model of Ezato et al. [49] reproduces the measured locations of homogeneous ignition and the ensuing flame shapes. The other two models fail to capture homogenous ignition [28], since their enhanced turbulent transport leads to increased upstream catalytic conversion that deprives hydrogen from the homogeneous pathway. Predicted transverse hydrogen profiles in Fig. 12a at the post-homogeneous-ignition location $x = 195$ mm for Cases 2 and 3 indicate that, even well-downstream of homogeneous ignition, the catalytic pathway may still convert hydrogen in parallel

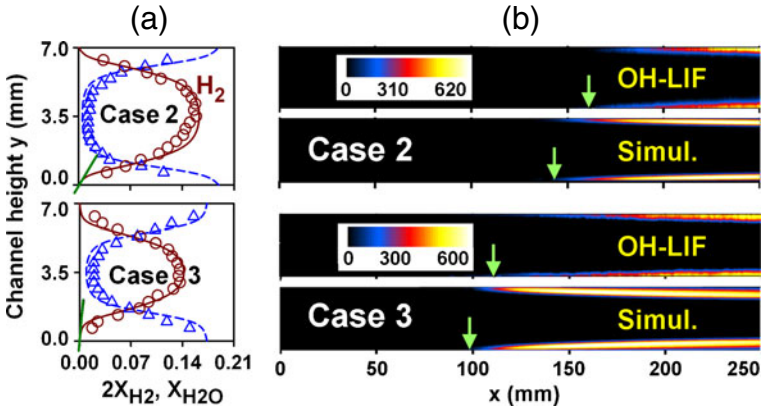

Fig. 12 **a** Raman-measured (*symbols*) and numerically predicted (*lines*, using the LR model of Ezato et al. [49]) transverse profiles of species mean mole fractions for Case 2 (operating conditions shown in the legend of Fig. 11) and Case 3 ($\varphi = 0.24$, $U_{\text{IN}} = 20$ m/s, $Re_{\text{IN}} = 15{,}080$) at $x = 195$ mm: H_2: *circles* and *solid lines*, H_2O: *triangles* and *dashed lines*. **b** LIF-measured and predicted (using the Ezato et al. [49] model) distributions of the OH radical for Cases 2 and 3. The *arrows* indicate the onset of homogeneous ignition and the *color bars* the predicted OH levels in ppmv. Adapted from [28]

to the gaseous pathway. For the higher Reynolds number Case 2, for example, the predicted transverse gradient of hydrogen at the wall (shown with the thick solid line in Fig. 12a) is non-zero, signifying fuel leakage through the flame zone. This is further supported by the Raman measurements despite near-wall limitations of the Raman experiments. Fuel leakage is insignificant in Case 3 (the transverse gradient of H_2 at the wall is nearly zero) due to its lower Reynolds number.

In conclusion, the interplay of transport (laminar or turbulent) with hetero-/homogeneous combustion is very rich in confined channel configurations. Homogeneous ignition chemistry, propagation characteristics, competition between the two reaction pathways for fuel consumption, diffusional imbalance of the limiting reactant, flow laminarization due to heat transfer from the catalytic walls and fuel leakage through the gaseous combustion zone are the controlling processes. The near-wall in situ thermoscalar and velocity measurements presented in this section are indispensable tools for understanding the underlying processes and validating advanced numerical models. In particular, key to understanding the near-wall heat and mass transfer processes would be the measurement of turbulent scalar fluxes, $\widetilde{u_i'\varphi'}$, with φ' denoting temperature or species mass fractions fluctuations. Such quantities would involve joint velocity-scalar measurements near the catalytic surface. In terms of modeling, direct numerical simulation (DNS) at moderate (but still realistic) Reynolds numbers is nowadays feasible in practical geometries (catalytic channel hydraulic diameters of $\sim$1 mm and lengths of 30 to 75 mm [3]) and can complement the turbulent scalar flux measurements. The DNS numerical tool discussed in the coming Section 4.3 can be used for turbulent channel catalytic combustion. Finally, 3-D DNS has recently been reported in turbulent channel catalytic combustion (pure heterogeneous chemistry) of lean H_2/air mixtures [56]. This study identified the origin of flow laminarization (suppression of vorticity components parallel to the wall) and assessed the magnitude of the catalytic reaction rate fluctuations. Extension of [56] to 3-D turbulent DNS with combined heterogeneous and homogeneous chemistry is under way.

4.3 Transient hetero-/homogeneous combustion

The dynamic behavior of catalytic combustion systems involves complex interactions of hetero-/homogeneous kinetics, fluid transport, and heat conduction in the solid walls. Transient behavior is manifested not only because of change in reactor operating conditions (as, for example, injection of fuel during catalytic ignition or variation in mass throughput during engine load control) but also due to intrinsic dynamics driven by interactions between heterogeneous and/or homogeneous chemistry, transport, and solid walls. The flow is still laminar and, contrary to the transient but statistically-steady turbulent combustion results of Section 4.2, the mean thermoscalar and flow field can vary in time. Light-off studies of methane-fueled catalytic microreactors are firstly presented, followed by investigation of dynamical behavior in hydrogen-fueled catalytic reactors. Appropriate numerical tools and allowed model simplifications as well as guidelines for temporally-resolved in situ measurements are given.

Modeling of light-off is presented for methane-fueled catalytic microreactors at pressures of 3 to 5 bar and reactant preheats of 850 K (operating conditions relevant to recuperated microturbine-based power systems [2]). A plane channel

configuration similar to that in Fig. 1 is considered, having 10 mm length, 1 mm height (H) and 50 μm solid wall thickness; the initial 1 mm is catalytically inert and the remaining 9 mm length is coated with platinum [57]. While still keeping a spatially multidimensional description (2-D in this case), for reasons elaborated in Section 3, simplifications are sought to the full transient treatment in Eqs. 1 to 10. This is due to the particularly long times required to achieve steady state, dictated by the large thermal inertia of the solid. The quasisteady treatment of the gas-phase processes (transport and chemistry) and surface chemistry offers such a possibility; this is a result of disparity between the gas-phase transport and gas/surface chemical time scales from the one side and the solid-phase heat conduction time scale from the other side. To this direction, all transient terms can be dropped in the governing equations except for the solid heat conduction (Eq. 9).

While the validity of the quasisteady assumption in terms of convective and diffusive flow time scales is rather straightforward to assess, the corresponding validity in terms of chemical time scales has not received proper attention. Application of the quasisteady model to the aforementioned microreactor geometry has been performed in [57], using the methane hetero-/homogeneous reaction schemes validated in Section 4.1. Figure 13b provides computed characteristic chemical times for species conversion (combined catalytic and gas-phase) at various temperatures. For the present microreactor application with a high preheat of 850 K, the quasisteady assumption is valid for solid integration times of 50 ms. This integration time is short enough to resolve heat conduction in the solid and long enough to ensure applicability of the quasisteady assumption. Figure 13a provides predicted 2-D maps of CH_4 and OH at three times, spanning from light-off ($t = 11.5$ s) to steady state ($t = 26.4$ s). Although the reactor starts as a catalytic one, at steady state it practically becomes

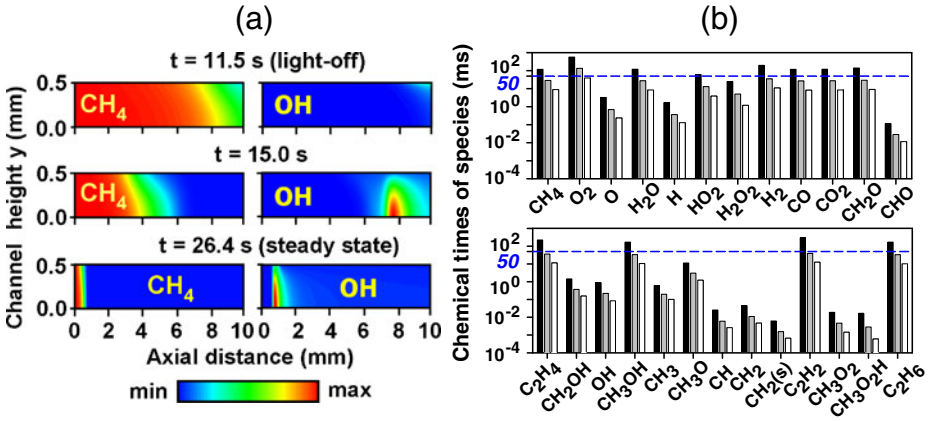

Fig. 13 **a** Computed 2-D distributions of CH_4 and OH mass fractions at three time instances during catalytic microreactor start-up: plane channel geometry with 10 mm length and 1 mm height ($y = 0$ is the symmetry plane and $y = 0.5$ mm the gas-wall interface), $\varphi = 0.40$, $p = 5$ bar, $U_{IN} = 0.3$ m/s. The scaling in the color bar corresponds to the ranges: CH_4: 0.0 to 0.022, OH: 0.0 to 0.59×10^{-6} ($t = 11.5$ s), 59×10^{-6} ($t = 15.0$ s) and 766×10^{-6} ($t = 26.4$ s). **b** Computed gas-phase species characteristic chemical times in CH_4/air combustion ($\varphi = 0.40$) over Pt. Initial temperatures: 750 K (*black bars*), 800 K (*gray bars*) and 850 K (*white bars*). The horizontal dashed line at 50 ms defines the time step used for the integration of the solid heat conduction equation (adapted from [57])

a homogeneous reacting system since the flame is anchored slightly upstream of the catalytically-coated section ($x = 1$ mm). While such quasisteady model predictions have been successfully used to reproduce transient experiments in practical reactors (e.g. catalytic partial oxidation studies in [58]), care must be exercised when the initial gas temperatures are low enough. The chemical time scales before light-off may then become commensurable or longer than the solid heat conduction time. This would invalidate the quasisteady formulation and necessitate the full transient solution of Eqs. 1–10 (direct numerical simulation), a particularly demanding task given the particularly long integration times necessary to reach steady state (tens of seconds, see Fig. 13a).

Full transient models (direct numerical simulations) may also be necessary in case of intrinsic flame dynamics. Channel flow combustion is known to exhibit a wealth of dynamical behaviors. Direct numerical simulation of flame dynamics in H_2-fueled, Pt-coated catalytic channels with prescribed wall temperature ($= 960$ K) and detailed hetero-/homogeneous chemistry has recently been performed in [59, 60], extending parallel work in inert (non-catalytic) channels [61–63]. Computed flame modes are investigated as a function of the inflow velocity, U_{IN}, and the catalytic reactivity. The latter is controlled by the ratio of the active-to-geometrical surface area, B, which is the parameter discussed in Eqs. 8 and 10 ($B = 0$ denotes a non-catalytic channel). The flame dynamics for an $H = 2$ mm channel height are presented in Fig. 14b for four values of the catalytic reactivity parameter B. To facilitate the graphical presentation of all flame solutions, the parameter h_{Tmax} has been defined in the vertical axis of Fig. 14b: it denotes the transverse distance from the lower channel wall ($y = 0$) to the point of the maximum temperature, normalized by the channel height H.

In technical systems with a well-dispersed catalyst, B is larger than unity such that the catalytic conversion rates of the typically less-reactive hydrocarbon fuels are enhanced. However, because of the very high reactivity of H_2 on platinum, transport-limited catalytic conversion is already attested at $B = 1$. Therefore, effects of finite-rate surface chemistry on the flame dynamics are investigated by reducing B to suitably low values ($3.0 \times 10^{-3} \leq B \leq 1.75 \times 10^{-2}$). Such values can be realized in practice by a very low loading of Pt on the catalyst washcoat. The steady and unsteady flame modes for the inert case ($B = 0$) are shown in Fig. 14b and their sequence with increasing U_{IN} is: steady mild combustion, repetitive (oscillatory) ignition/extinction, steady closed symmetric, oscillating, steady open symmetric, and finally steady upper or lower asymmetric flames.

The lowest examined catalytic reactivity $B = 0.003$ suppresses the mild combustion mode while the oscillatory ignition/extinction modes are suppressed for $B \geq 0.0175$. Typical oscillatory flame solutions for $B = 0.005$ are shown in Fig. 14a. In terms of the asymmetric modes, with increasing catalytic reactivity (B) the flames become progressively less asymmetric but it is still not possible to restore full symmetry. The frequency of the unsteady modes, for the 2 mm channel height, range from a few tens of Hz (repetitive ignition extinction) to hundreds of Hz (oscillatory flames), clearly showing the necessity of a full transient simulation (Eqs. 1–10). To aid in complexity, the heterogeneous pathway can also have its own intrinsic dynamics [64]. The presence of catalytically-driven dynamics, their potential coupling with homogeneous-driven dynamics, and finally their response to time-varying reactor operating conditions (ignition, load change etc.) require full transient (DNS) models

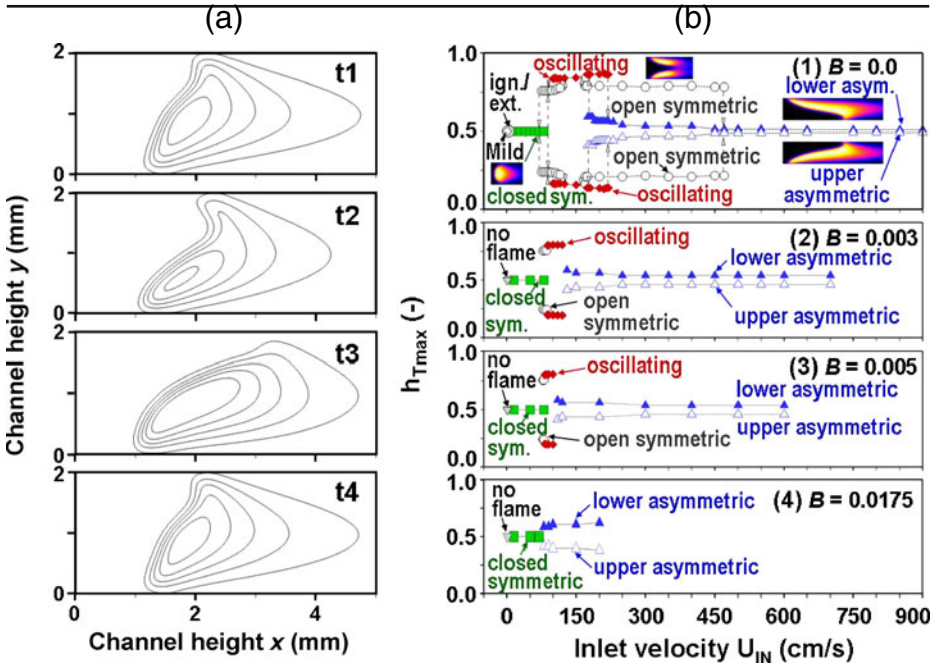

Fig. 14 **a** Oscillating flame in a 2 mm height channel for $U_{IN} = 100$ cm/s and catalytic reactivity parameter $B = 0.005$: five Y_{OH} isolines (in the range $0.0007 \leq Y_{OH} \leq 0.0034$) at four time instants spanning a full period of oscillation. **b** Combustion modes as a function of inlet velocity U_{IN} and catalytic reactivity B for an $H = 2$ mm height channel. The images for $B = 0$ (inert channel walls) provide typical flame shapes of various combustion modes via the distributions of the OH radical mass fraction at the flame vicinity (adapted from [59, 60])

with inclusion of heat transfer in the solid wall. Such advanced models can be used for fundamental hetero-/homogeneous combustion studies and for design of practical reactors. The 2-D [59–62] and 3-D [63] DNS models employed to study flame dynamics in catalytic and non-catalytic channels are presently modified for inclusion of heat conduction in the solid walls.

In situ measurements are also essential tools for transient studies. Initial measurements of flame dynamics in the optically accessible reactor of Fig. 2 using high speed (2 kHz) flame chemiluminescence imaging during combustion of syngas (CO/H_2) over non-catalytic walls have recently been reported in [65]. Extending the in situ measuring techniques to high speed LIF and Raman appears feasible. Contrary to open turbulent flame diagnostics, whereby measurements at rates of tens of kHz are needed to temporally resolve strongly turbulent motions, heterogeneous and homogeneous intrinsic dynamics in channel flows of practical confinements rarely exceed 1 kHz. The combination of advanced in situ temporally-resolved measurements and DNS is thus expected to substantially grow in the coming years.

5 Conclusions

It has been demonstrated that multidimensional numerical modeling and in situ spatially-resolved measurements of gas-phase thermoscalars over the catalyst

boundary layer can advance the fundamental investigation of heterogeneous and homogeneous chemical reaction schemes and their coupling at industrially-relevant operating conditions. The procedure for validating catalytic and gas-phase reaction mechanisms has been presented for the combustion of various practical fuels over polycrystalline platinum. Furthermore, the combination of advanced modeling and in situ near-wall measurements of thermoscalars and velocity has clarified the intricate interplay of interphase fluid transport (laminar or turbulent) and hetero-/homogeneous kinetics. Homogeneous ignition chemistry, flame propagation characteristics, competition between the two reaction pathways for fuel consumption, diffusional imbalance of the limiting reactant, flow laminarization due to heat transfer from the catalytic walls and fuel leakage through the gaseous combustion zone are the controlling processes. Recent DNS in turbulent catalytic combustion has clarified the origin of flow laminarization and assessed the magnitude of catalytic reaction rate fluctuations.

Dynamic behavior driven by interactions between homogeneous chemistry and solid walls has been subsequently demonstrated using detailed transient simulation (laminar DNS) in channel geometries. It is shown that the presence of catalytic reactions on the walls moderates homogeneous-kinetic-driven instabilities; however, depending on the catalytic reactivity and operating conditions, such dynamics can still persist in the form of oscillatory modes in practical catalytic reactors. Computer power is nowadays sufficient for application of advanced multidimensional transient models to gain insight on catalytically-driven dynamics, their potential coupling with homogeneous-kinetics-driven dynamics, and finally their response to time-varying reactor operating conditions (ignition, load change etc.). For this purpose, temporally-resolved in situ measurements of thermoscalars over the catalyst surfaces are necessary to complement the simulations. This approach could also greatly facilitate the development of start-up procedures and well-defined operational envelopes in order to circumvent unstable reactor combustion modes in industrial reactors.

Acknowledgements Support was provided by the Swiss National Science Foundation (SNF), the Swiss Federal Office of Energy (BfE), the Swiss Competence Center for Energy and Mobility (CCEM) via project Carbon Management and the European Union via project H_2-IGCC.

References

1. Karagiannidis, S., Mantzaras, J., Jackson, G., Boulouchos, K.: Hetero-/homogeneous combustion and stability maps in methane-fueled microreactors. Proc. Combust. Inst. **31**, 3309–3317 (2007)
2. Schneider, B., Karagiannidis, S., Bruderer, M., Dyntar, D., Zwyssig, C., Guangchun, Q., Diener, M., Boulouchos, K., Abhari, R.S., Guzzella, L., Kolar, J.W.: Ultra-high-energy-density converter for portable power. Paper presented at the Power-MEMS 2005, Tokyo, Japan, 28–30 Nov 2005
3. Carroni, R., Griffin, T., Mantzaras, J., Reinke, M.: High-pressure experiments and modeling of methane/air catalytic combustion for power-generation applications. Catal. Today **83**(1–4), 157–170 (2003)
4. Griffin, T., Winkler, D., Wolf, M., Appel, C., Mantzaras, J.: Staged catalytic combustion method for the advanced zero emissions gas turbine power plant. ASME, paper No. 2004-54101 (2004)
5. Christmann, K., Freund, H.J., Kim, J., Koel, B., Kuhlenbeck, H., Morgenstern, M., Panja, C., Pirug, G., Rupprechter, G., Samano, E., Somorjai, G.A.: Adsorption of molecules on metal, semiconductor and oxide surfaces. Landolt-Bornstein: Numerical Data and Functional Relationships in Science and Technology - New Series, Springer Verlag, New York (2006)

6. Singh, J., Nelson, R.C., Vicente, B.C., Scott, S.L., van Bokhoven, J.: Electronic structure of alumina-supported monometallic Pt and bimetallic PtSn catalysts under hydrogen and carbon monoxide environment. Phys. Chem. Chem. Phys. **12**(21), 5668–5677 (2010)
7. Griffin, T.A., Calabrese, M., Pfefferle, L.D., Sappey, A., Copeland, R., Crosley, D.R.: The influence of catalytic activity on the ignition of boundary-layer flows 3. Hydroxyl radical measurements in low- pressure boundary-layer flows. Combust. Flame **90**(1), 11–33 (1992)
8. Dogwiler, U., Mantzaras, J., Benz, P., Kaeppeli, B., Bombach, R., Arnold, A.: Homogeneous ignition of methane/air mixtures over platinum: comparison of measurements and detailed numerical predictions. Proc. Combust. Inst. **27**, 2275–2282 (1998)
9. Appel, C., Mantzaras, J., Schaeren, R., Bombach, R., Inauen, A., Kaeppeli, B., Hemmerling, B., Stampanoni, A.: An experimental and numerical investigation of homogeneous ignition in catalytically stabilized combustion of hydrogen/air mixtures over platinum. Combust. Flame **128**(4), 340–368 (2002)
10. Reinke, M., Mantzaras, J., Schaeren, R., Bombach, R., Inauen, A., Schenker, S.: High-pressure catalytic combustion of methane over platinum: in situ experiments and detailed numerical predictions. Combust. Flame **136**(1–2), 217–240 (2004)
11. Reinke, M., Mantzaras, J., Bombach, R., Schenker, S., Inauen, A.: Gas phase chemistry in catalytic combustion of methane/air mixtures over platinum at pressures of 1 bar to 16 bar. Combust. Flame **141**, 448–468 (2005)
12. Pfefferle, W.C., Pfefferle, L.D.: Catalytically stabilized combustion. Prog. Energy Combust. Sci. **12**(1), 25–41 (1986)
13. Dogwiler, U., Benz, P., Mantzaras, J.: Two-dimensional modelling for catalytically stabilized combustion of a lean methane-air mixture with elementary homogeneous and heterogeneous chemical reactions. Combust. Flame **116**(1–2), 243–258 (1999)
14. Mantzaras, J., Benz, P.: An asymptotic and numerical investigation of homogeneous ignition in catalytically stabilized channel flow combustion. Combust. Flame **119**(4), 455–472 (1999)
15. Mantzaras, J., Appel, C.: Effects of finite rate heterogeneous kinetics on homogeneous ignition in catalytically stabilized channel flow combustion. Combust. Flame **130**(4), 336–351 (2002)
16. Andrae, J.C.G., Björnbom, P.H.: Wall effects of laminar hydrogen flames over platinum and inert surfaces. AICHE J. **46**, 1454–1460 (2000)
17. Bui, P.A., Vlachos, D.G., Westmoreland, P.R.: Homogeneous ignition of hydrogen/air mixtures over platinum. Proc. Combust. Inst. **26**, 1763–1770 (1996)
18. Reinke, M., Mantzaras, J., Bombach, R., Schenker, S., Tylli, N., Boulouchos, K.: Effects of H_2O and CO_2 dilution on the catalytic and gas-phase combustion of methane over platinum at elevated pressures. Combust. Sci. Technol. **179**, 553–600 (2006)
19. Groppi, G., Ibashi, W., Tronconi, E., Forzatti, P.: Structured reactors for kinetic measurements under severe conditions in catalytic combustion over palladium supported systems. Catal. Today **69**(1–4), 399–408 (2001)
20. Lyubovsky, M., Pfefferle, L.: Complete methane oxidation over Pd catalyst supported on alpha-alumina. Influence of temperature and oxygen pressure on the catalyst activity. Catal. Today **47**(1–4), 29–44 (1999)
21. Song, X., Williams, W.R., Schmidt, L.D., Aris, R.: Bifurcation behavior in homogeneous-heterogeneous combustion: 2. Computations for stagnation-point flow. Combust. Flame **84**(3–4), 292–311 (1991)
22. Deutschmann, O., Schmidt, R., Behrendt, F., Warnatz, J.: Numerical modeling of catalytic ignition. Proc. Combust. Inst. **26**, 1747–1754 (1996)
23. Aghalayam, P., Park, Y.K., Vlachos, D.G.: A detailed surface reaction mechanism for CO oxidation on Pt. Proc. Combust. Inst. **28**, 1331–1339 (2000)
24. Sidwell, R.W., Zhu, H.Y., Kee, R.J., Wickham, D.T.: Catalytic combustion of premixed methane-in-air on a high-temperature hexaaluminate stagnation surface. Combust. Flame **134**(1–2), 55–66 (2003)
25. Ghermay, Y., Mantzaras, J., Bombach, R.: Effects of hydrogen preconversion on the homogeneous ignition of fuel lean $H_2/O_2/N_2/CO_2$ mixtures over platinum at moderate pressures. Combust. Flame **157**, 1942–1958 (2010)
26. Ghermay, Y., Mantzaras, J., Bombach, R.K.B.: Homogeneous combustion of fuel lean $H_2/O_2/N_2$ mixtures over platinum at elevated pressures and preheats. Combust. Flame **158**, 1491–1506 (2011)

27. Ghermay, Y., Mantzaras, J., Bombach, R.: Experimental and numerical investigation of hetero-/homogeneous combustion of $CO/H_2/O_2/N_2$ mixtures over platinum at pressures up to 5 bar. Proc. Combust. Inst. **33**, 1827–1835 (2011)
28. Appel, C., Mantzaras, J., Schaeren, R., Bombach, R., Inauen, A.: Turbulent catalytically stabilized combustion of hydrogen/air mixtures in entry channel flows. Combust. Flame **140**, 70–92 (2005)
29. Groppi, G., Belloli, A., Tronconi, E., Forzatti, P.: A comparison of lumped and distributed models of monolith catalytic combustors. Chem. Eng. Sci. **50**(17), 2705–2715 (1995)
30. Mantzaras, J., Appel, C., Benz, P.: Catalytic combustion of methane/air mixtures over platinum: homogeneous ignition distances in channel flow configurations. Proc. Combust. Inst. **28**, 1349–1357 (2000)
31. Kee, R.J., Dixon-Lewis, G., Warnatz, J., Coltrin, M.E., Miller, J.A.: A Fortran computer code package for the evaluation of gas-phase multicomponent transport properties. In. Sandia National Laboratories Report No. SAND86-8246, Livermore, USA (1996)
32. Mladenov, N., Koop, J., Tischer, S., Deutschmann, O.: Modeling of transport and chemistry in channel flows of automotive catalytic converters. Chem. Eng. Sci. **65**, 812–826 (2010)
33. Sinha, N., Bruno, C., Bracco, F.V.: Two-dimensional, transient catalytic combustion of CO-air on platinum. Physicochem. Hydrodyn. **6**(4), 373–391 (1985)
34. Deutschmann, O., Maier, L.I., Riedel, U., Stroemman, A.H., Dibble, R.W.: Hydrogen assisted catalytic combustion of methane on platinum. Catal. Today **59**(1–2), 141–150 (2000)
35. Warnatz, J., Dibble, R.W., Maas, U.: Combustion, Physical and Chemical Fundamentals, Modeling and Simulation. Springer-Verlag, New York (1996)
36. Reinke, M., Mantzaras, J., Schaeren, R., Bombach, R., Kreutner, W., Inauen, A.: Homogeneous ignition in high-pressure combustion of methane/air over platinum: comparison of measurements and detailed numerical predictions. Proc. Combust. Inst. **29**, 1021–1029 (2002)
37. Smith, G.P., Golden, D.M., Frenklach, M., Moriarty, N.W., Eiteneer, B., Goldenberg, M., Bowman, C.T., Hanson, R.K., Song, S., Gardiner, W.C., Lissianski, V., Qin, Z.: An optimized detailed chemical reaction mechanism for methane combustion. In: Gas Research Institute (2000)
38. Hughes, K.J., Turanyi, T., Clague, A., Pilling, M.J.: Development and testing of a comprehensive chemical mechanism for the oxidation of methane. Int. J. Chem. Kinet. **33**, 513–538 (2001)
39. Reinke, M., Mantzaras, J., Schaeren, R., Bombach, R., Inauen, A., Schenker, S.: Homogeneous ignition of CH_4/air and H_2O- and CO_2-diluted CH_4/O_2 mixtures over platinum; an experimental and numerical investigation at pressures up to 16 bar. Proc. Combust. Inst. **30**, 2519–2527 (2005)
40. Karagiannidis, S., Mantzaras, J., Schenker, S., Boulouchos, K.: Experimental and numerical investigation of the hetero-/homogeneous combustion of lean propane/air mixtures over platinum. Proc. Combust. Inst. **32**, 1947–1955 (2009)
41. Garetto, T.F., Rincon, E., Apesteguia, C.R.: Deep oxidation of propane on Pt-supported catalysts: drastic turnover rate enhancement using zeolite supports. Appl. Catal. B-Environ. **48**, 167–174 (2004)
42. Qin, Z., Lissianski, V.V., Yang, H., Gardiner, W.C., Davis, S.G., Wang, H.: Combustion chemistry of propane: a case study of detailed reaction mechanism optimization. Proc. Combust. Inst. **28**, 1663–1669 (2000)
43. Mueller, M.A., Kim, T.J., Yetter, R.A., Dryer, F.L.: Flow reactor studies and kinetic modeling of the H_2/O_2 reaction. Int. J. Chem. Kinet. **31**(2), 113–125 (1999)
44. Miller, J.A., Bowman, C.T.: Mechanism and modeling of nitrogen chemistry in combustion. Prog. Energ. Combust. **15**(4), 273–338 (1989)
45. Mantzaras, J., Bombach, R., Schaeren, R.: Hetero-/homogeneous combustion of hydrogen/air mixtures over platinum at pressures up to 10 bar. Proc. Combust. Inst. **32**, 1937–1945 (2009)
46. Li, J., Zhao, Z., Kazakov, A., Dryer, F.L.: An updated comprehensive kinetic model of hydrogen combustion. Int. J. Chem. Kinet. **36**, 566–575 (2004)
47. Glassman, I.: Combustion, 3rd edn. Academic Press, London (1996)
48. Mantzaras, J.: Catalytic combustion of syngas. Combust. Sci. Technol. **180**, 1137–1168 (2008)
49. Ezato, K., Shehata, A.M., Kunugi, T., McEligot, D.M.: Numerical prediction of transitional features of turbulent forced gas flows in circular tubes with strong heating. ASME Transactions Journal of Heat Transfer **121**(3), 546–555 (1999)
50. Satake, S., Kunugi, T., Shehata, A.M., McEligot, D.M.: Direct numerical simulation for laminarization of turbulent forced gas flows in circular tubes with strong heating. Int. J. Heat Fluid Flow **21**(5), 526–534 (2000)

51. Mantzaras, J., Appel, C., Benz, P., Dogwiler, U.: Numerical modelling of turbulent catalytically stabilized channel flow combustion. Catal. Today **59**(1–2), 3–17 (2000)
52. Appel, C., Mantzaras, J., Schaeren, R., Bombach, R., Kaeppeli, B., Inauen, A.: An experimental and numerical investigation of turbulent catalytically stabilized channel flow combustion of hydrogen/air mixtures over platinum. Proc. Combust. Inst. **29**, 1031–1038 (2002)
53. Chen, H.C., Patel, V.C.: Near-wall turbulence models for complex flows including separation. AIAA J. **26**(6), 641–648 (1988)
54. Hwang, C.B., Lin, C.A.: Improved low-Reynolds-number k-ε model based on direct numerical simulation data. AIAA J. **36**(1), 38–43 (1998)
55. Liu, Z.C., Landreth, C.C., Adrian, R.J., Hanratty, T.J.: High resolution measurement of turbulent structure in a channel with particle image velocimetry. Exp. Fluids **10**, 301–312 (1991)
56. Lucci, F., Frouzakis, C.E., Mantzaras, J.: Three-dimensional direct numerical simulation of turbulent catalytic combustion of hydrogen over platinum. Proc. Combust. Inst. **34**, 2295–2302 (2013)
57. Karagiannidis, S., Mantzaras, J.: Numerical investigation on the start-up of methane-fueled catalytic microreactors. Combust. Flame **157**, 1400–1413 (2010)
58. Schneider, A., Mantzaras, J., Eriksson, S.: Ignition and extinction in catalytic partial oxidation of methane-oxygen mixtures with large H_2O and CO_2 dilution. Combust. Sci. Technol. **180**, 89–126 (2008)
59. Pizza, G., Mantzaras, J., Frouzakis, C.E., Tomboulides, A.G., Boulouchos, K.: Suppression of combustion instabilities of premixed hydrogen/air flames in microchannels using heterogeneous reactions. Proc. Combust. Inst. **32**, 3051–3058 (2009)
60. Pizza, G., Mantzaras, J., Frouzakis, C.E.: Flame dynamics in catalytic and non-catalytic mesoscale microreactors. Catal. Today **155**, 123–130 (2010)
61. Pizza, G., Frouzakis, C.E., Mantzaras, J., Tomboulides, A.G., Boulouchos, K.: Dynamics of premixed hydrogen/air flames in microchannels. Combust. Flame **152**(3), 433–450 (2008)
62. Pizza, G., Frouzakis, C.E., Mantzaras, J., Tomboulides, A.G., Boulouchos, K.: Dynamics of premixed hydrogen/air flames in mesoscale channels. Combust. Flame **155**(1–2), 2–20 (2008)
63. Pizza, G., Frouzakis, C.E., Mantzaras, J., Tomboulides, A.G., Boulouchos, K.: Three-dimensional simulations of premixed hydrogen/air flames in micro tubes. J. Fluid. Mech. **658**, 463–491 (2010)
64. Slinko, M.M., Jaeger, N.I.: Oscillatory Heterogeneous Catalytic Systems, vol. 86. Studies in Surface Science and Catalysis, Elsevier, Amsterdam (1994)
65. Brambilla, A., Ghermay, Y., Frouzakis, C.E., Mantzaras, J., Bombach, R.: Experimental and numerical investigation of combustion dynamics in lean premixed CO/H_2/air mixtures in a mesoscale channel. Paper presented at the 13th international conference on numerical combustion, Corfu, Greece, 27–29 April 2011